J. Phys. Chem. A **2009,** *113,* 3387–3394 **3387**

Experimental and Theoretical Study of Hydrogen Thiocarbonate for Heterogeneous Reaction of Carbonyl Sulfide on Magnesium Oxide

Yongchun Liu and Hong He*

Research Center for Eco-Environmental Sciences, Chinese Academy of Sciences, Beijing 100085, China

Received: November 10, 2008; Revised Manuscript Received: January 9, 2009

In situ diffuse reflectance infrared Fourier transform spectroscopy combined with derivative spectroscopy analysis, two-dimensional correlation spectroscopy analysis, and quantum chemical calculations were used to investigate the infrared absorbance assignment and the molecular structure of hydrogen thiocarbonate on magnesium oxide. The bands at 1283 and 1257 cm^{-1}, which had the typical characteristic of intermediate, were observed in experiments for the heterogeneous reaction of COS on MgO. On the basis of two-dimensional correlation spectroscopy analysis and quantum chemical calculations, the band at 1283 cm^{-1} was assigned to the υ_s band of bridged thiocarbonate which formed on the two neighboring Mg atoms in the (100) face of MgO crystal, and the band at 1257 cm^{-1} was the υ_s band of monodentate thiocarbonate on MgO. The υ_{as}(OCO) band of thiocarbonates was invisible in the experiment due to their weak absorbance and the interruption of surface carbonate. The formation mechanism of thiocarbonates is proposed, which occurred through a nucleophilic attack of preadsorbed COS by surface −OH groups followed by hydrogen atom transfer from the −OH group to the sulfur atom of preadsorbed COS. The activation energy for the intramolecular proton-transfer reaction of bridged thiocarbonate was calculated to be 18.52 kcal·mol^{-1} at the B3LYP/6-31+G(d,p) level of theory.

1. Introduction

In the past decades, much attention was drawn to the sources and sinks of carbonyl sulfide (COS) in the atmosphere due to the important role of COS in the formation of stratospheric sulfate aerosols (SSA).[1−5] Several modeling studies have shown that atmospheric particles often act as a sink for certain species.[6,7] Mineral dust with an annual emission of about 1000−3000 Tg represents one of the largest natural mass fractions of atmospheric particles.[7] It suggests that heterogeneous reactions on mineral dust may be a new sink of COS in the atmosphere. Recently, a few studies demonstrated that heterogeneous hydrolysis and oxidation of COS on mineral oxides, such as Al_2O_3, Fe_2O_3, CaO, MgO, and MnO_2, can take place under ambient conditions.[8−15] For example, the true initial uptake coefficient and steady-state uptake coefficient of COS on α-Al_2O_3 at 300 K were measured to be $(3.8 \pm 0.8) \times 10^{-7}$ and $(6.5 \pm 2.49) \times 10^{-8}$, respectively;[14] the corresponding uptake coefficients of COS on MgO were measured to be $(4.84 \pm 0.60) \times 10^{-7}$ and $(1.68 \pm 0.41) \times 10^{-7}$.[15] The reaction mechanism of COS on mineral oxides can be summarized as shown in eq 1[10−15]

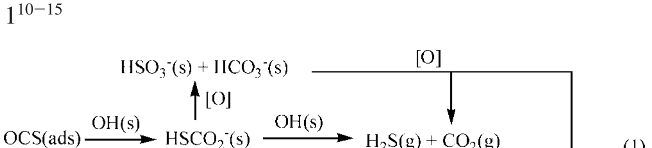

(1)

In eq 1, gaseous carbon dioxide (CO_2), hydrogen sulfide (H_2S),[12,14,15] and sulfur dioxide (SO_2) and surface sulfite (SO_3^{2-}) and sulfate (SO_4^{2-}) were found to be the gaseous and surface products, respectively. Hydrogen thiocarbonate ($HSCO_2^-$, HTC) was proposed to be the crucial intermediate for both the oxidation and the hydrolysis pathway. Therefore, it is significant to investigate the structure and properties of HTC on mineral oxides.

As for HTC on Al_2O_3, Hoggan et al.[16] observed the vibrational frequency of υ_{as}(OCO) and υ_s(OCO) in $HSCO_2^-$ at 1572 and 1327 cm^{-1}, respectively, using Fourier transform infrared spectroscopy (FTIR). However, we only observed the υ_{as}(OCO) band at 1574 cm^{-1} on Al_2O_3 using in situ diffuse reflectance infrared Fourier transform spectroscopy (in situ DRIFTS).[10,11] On the other hand, the infrared band of HTC on MgO was found to be much different from that of HTC on Al_2O_3. The band at 1273 cm^{-1} was ascribed to υ_s(OCO) of HTC on MgO.[12] As described in eq 1, many gaseous and surface species are present in the heterogeneous reaction of COS on mineral oxides. Therefore, their absorption bands may overlap each other. For example, the absorption bands for δ_{ip}(COH) of H_2CO_3, υ_{as}(COO$^-$) of bidentate and bridged carbonates are very close to 1273 cm^{-1};[17−20] SO_4^{2-} may also contribute the band at 1250 cm^{-1}.[21] The bands at 1574 and 1327 cm^{-1} may also originate from surface carbonate[22] and physisorbed SO_2,[23,24] respectively. Therefore, the assignment of infrared absorbance and molecular structure of HTC on mineral oxides need to be further carefully confirmed.

On the other hand, the signal-to-noise ratio of Al_2O_3 is very bad below 1200 cm^{-1} due to the strong lattice vibrational absorbance. Compared with Al_2O_3, MgO is more transparent for infrared. MgO is also one of the typical components in mineral aerosols and was widely used as a model oxide of environmental interface for the heterogeneous reactions of trace gases.[17] Therefore, the infrared assignment and the structure of HTC on MgO were systematically investigated using in situ DRIFTS, two-dimensional correlation spectroscopy (2DCOS), and density functional theory (DFT) calculations in this study.

---

* Corresponding author. Phone: +86-10-62849123. Fax: +86-10-62923563. E-mail: honghe@rcees.ac.cn.

10.1021/jp809887c CCC: $40.75

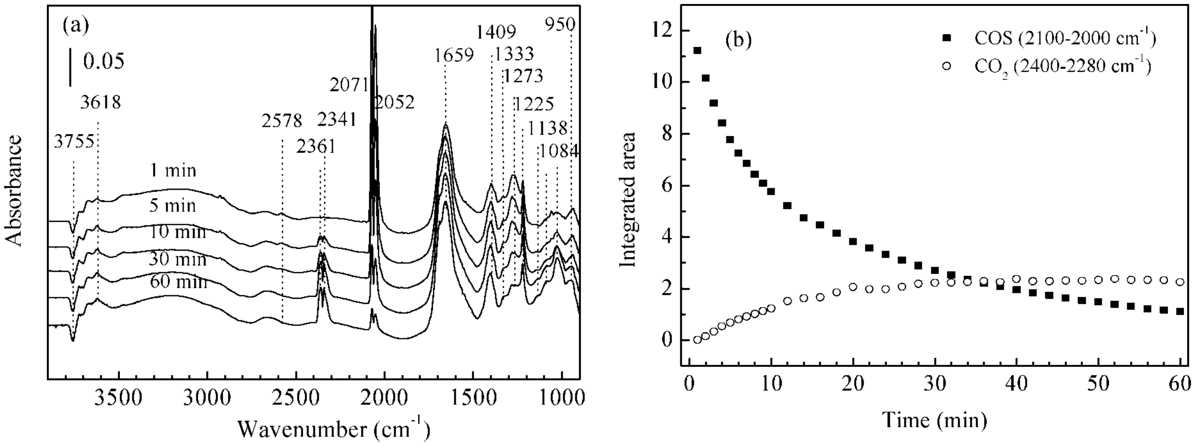

Figure 1. (a) Dynamic changes of in situ DRIFTS spectra in a closed system for MgO after exposure to 1000 ppmv of OCS/air at 303 K. (b) Dynamic changes of integrated areas for gaseous COS and CO_2.

The formation mechanism of HTC was also discussed. The results will further help in understanding the chemical process of COS taking place on mineral dust.

2. Experimental Section

2.1. Materials. MgO sample (A.R.) was supplied by Haizhong Chemical Plant in Tianjin. Its specific surface area was measured to be 14.6 $m^2 \cdot g^{-1}$ using nitrogen Brunauer−Emmett−Teller (BET) physisorption (Micromeritics ASAP 2000). The MgO sample was identified to be periclase with the three main 2θ peaks at 42.918°, 62.300°, and 78.622° by a D/max-RB automatic powder X-ray diffractometer (XRD) using Cu Kα irradiation. Carbonyl sulfide (COS, 2%, COS/N_2, Scott Specialty Gases Inc.) and N_2 and O_2 (99.999% purity, Beijing AP BEIFEN Gases Inc.) were used without further purification.

2.2. Experimental Methods. In situ DRIFTS spectra were recorded on a NEXUS 670 (Thermo Nicolet Instrument Corp.) FTIR, which was equipped with an in situ diffuse reflection chamber and a high sensitivity mercury cadmium telluride (MCT) detector cooled by liquid N_2. The infrared spectra were collected and analyzed by a computer with OMNIC 6.0 software. All spectra reported here were recorded at a resolution of 4 cm^{-1} for 100 scans. The volume of reactor chamber in the closed system was about 30 mL.

The MgO sample (about 10 mg) was finely ground and placed into a ceramic crucible in the in situ chamber. Before the DRIFTS measurement, the sample was pretreated in the in situ reactor chamber at 573 K in 100 $mL \cdot min^{-1}$ of simulated air stream (79% N_2 and 21% O_2) for 2 h. After the pretreated sample cooled to 303 K in simulated air, the reference spectrum was collected. COS (1000 ppmv) balanced with simulated air was introduced into the reactor for 3 min. Then, the inlet and outlet of reactor chamber were closed promptly. The infrared spectra in closed system were collected automatically by a computer. The relative humidity (RH) in the feed gases was measured to be 7 ± 1.5% with a hygrometer (Center 314).

2.3. Two-Dimensional Correlation Analysis. The collected spectra at equal time intervals of 1 min were selected for two-dimensional correlation analysis using “2D Pocha” software, which was developed by Daisuke Adachi (Kwansei Gakuin Univeristy).[25] A time-averaged reference spectrum was shown at the side and the top of the 2D correlation maps for comparison. In the 2D correlation maps, blue color regions denote positive correlation in intensity, while red color regions denote negative correlation in intensity.

2.4. Quantum Chemical Calculations. Quantum chemical calculations were performed to confirm the structure of $HSCO_2^-$ and assign its IR bands using a Gaussian 98 program.[26] Monodentate, bidentate, and bridged HTCs were built and are shown in Figure 5. Except for models VII and VIII, all geomety optimizations and vibrational frequency calculations of $HSCO_2^-$ on MgO were performed at the B3LYP hybrid DFT level of theory with 6-31+G(d,p) basis set. As for models VII and VIII, the bridged HTC was built on three-layer slabs of the MgO unit cell, and their geometries were optimized at the B3LYP/6-31G level of theory. To account for anharmonicity in the calculated vibrational frequencies, a scaling factor of 0.9632[27] was used. In the calculations of the proton-transfer mechanism of HTCs, geometry optimization and single point energy calculations of the transition state (TS) were also performed at B3LYP level of theory with 6-31+G(d,p) basis set.

3. Results and Discussion

3.1. Surface Species for the Heterogeneous Reaction of COS on MgO. Figure 1a shows the dynamic changes of in situ DRIFTS spectra at 303 K in the closed system. The changes of gaseous CO_2 and COS in intensities are also shown in Figure 1b. The absorbance band assignments in Figure 1a have been detailed in our previous work.[12] Obviously, the consumption of COS (2071 and 2052 cm^{-1}) and surface hydroxyl (3755 cm^{-1}) was observed. The products including gaseous CO_2 (2361 and 2341 cm^{-1}), surface bicarbonate (3618, 1659, 1409, and 1225 cm^{-1}), surface HS (2578 cm^{-1}), physically adsorbed SO_2 (1333 cm^{-1}), surface HSO_3^-/SO_3^{2-} (1084, 1030 and 945 cm^{-1}), and surface SO_4^{2-} (1138 cm^{-1}) could also be seen in Figure 1a. Compared with Al_2O_3,[10,11,16] apart from surface HSO_3^-, SO_3^{2-}, and SO_4^{2-}, the surface HS (2578 cm^{-1}) and the band of $HSCO_2^-$ around 1273 cm^{-1}, which will be discussed later, were also observed on MgO.

The spectra in the range of 1750−1150 cm^{-1} were very complicated. Derivative spectrum technology was very effective for qualitative and quantitative analysis of complex mixtures by infrared spectrometry.[28] Therefore, in order to enhance the spectrum resolution, the original spectrum at 10 min was analyzed with the second and the fourth derivative spectrum. The results are shown in Figure 2. Many shoulder peaks at 1693, 1632, 1578, 1497, 1283, and 1257 cm^{-1} are observed in Figure 2a. The very weak shoulder peaks at 1551, 1523, and 1365 cm^{-1} are also observed in Figure 2b. The band at 1693 cm^{-1} was assigned to ν(C=O) of carbonic acid (H_2CO_3).[19] It should be

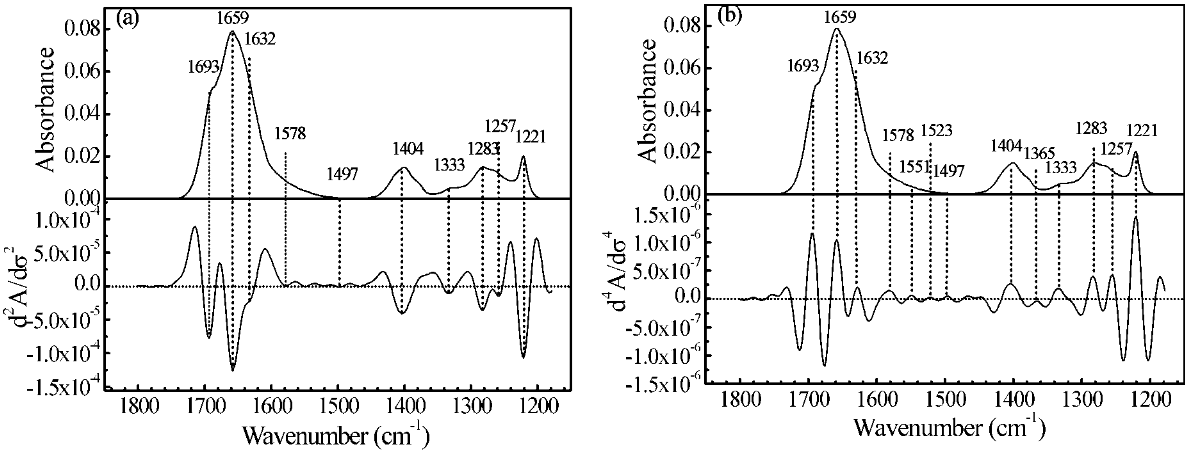

Figure 2. Derivative infrared spectra in the range of 1150−1750 cm^{-1} at 10 min: (a) the second derivative spectrum; (b) the fourth derivative spectrum.

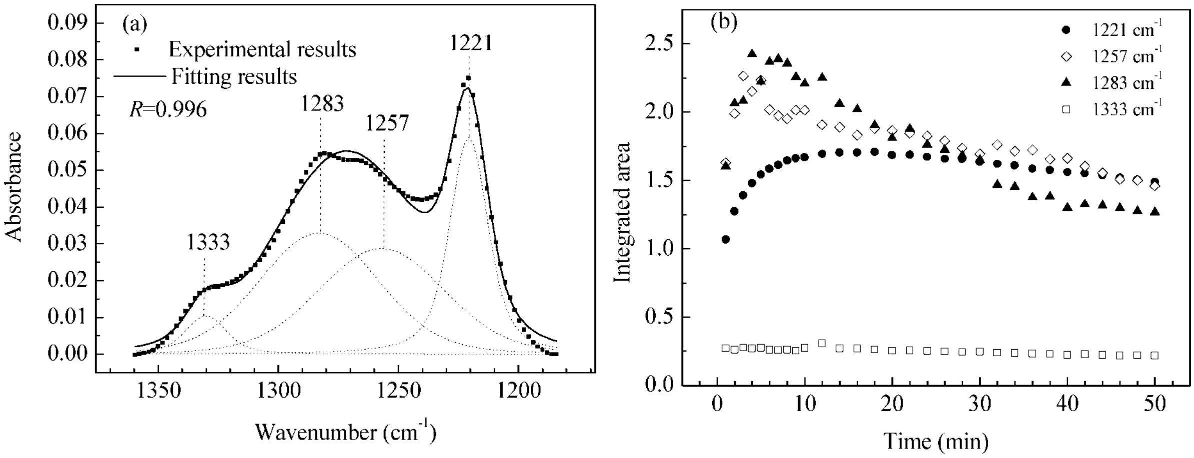

Figure 3. (a) Curve-fitting results for the spectrum at 10 min in the range of 1170−1360 cm^{-1}. (b) Dynamic changes of integrated areas for the bands at 1221, 1257, 1283, and 1333 cm^{-1}.

noted that bidentate carbonate may also contribute this band in the region of 1600−1670 cm^{-1}.[18] However, the band at 1693 cm^{-1} disappeared gradually when the reacted sample was purged in N_2 (not shown), which means it should not be related to carbonate species. The band at 1632 cm^{-1} was ascribed to δ(HOH) of absorbed H_2O,[29] which was accompanied by a broad peak v(OH) in the range of 3500−2800 cm^{-1} in Figure 1a. The bands in the region of 1530−1470 cm^{-1} were assigned to $v_{as}(COO^-)$ of monodentate carbonate.[20] The peak at 1365 cm^{-1} was due to the absorption band of surface SO_4^{2-}.[30] The bands at 1578 and 1551 cm^{-1} might also be related to surface carbonate.[22] It is worthwhile to note that the v_{as}(OCO) band of $HSCO_2^-$ at 1572 cm^{-1} on Al_2O_3[16] is very close to the peak at 1578 cm^{-1}. At the same time, the v_s(OCO) band of $HSCO_2^-$ at 1327 cm^{-1} [16] is also near the band at 1333 cm^{-1}, which was assigned to physically adsorbed SO_2 previously. The band around 1273 cm^{-1} in Figure 1a split into two bands at 1283 and 1257 cm^{-1} in Figure 2. As mentioned in the Introduction, the absorption bands for δ_{ip}(COH) of H_2CO_3, $v_{as}(COO^-)$ of bidentate and bridged carbonates are very close to the band around 1273 cm^{-1}, and SO_4^{2-} may also contribute to the band at 1250 cm^{-1}.[21] Therefore, the assignment for the bands at 1578, 1333, and around 1273 cm^{-1} need be further carefully confirmed.

3.2. Dynamic Analysis for the Surface Species. In order to clearly observe the dynamic changes of surface species and ascertain the assignment of the bands mentioned above, the spectra in the range of 1170−1360 cm^{-1} were fitted on the basis of the deconvolved curves. Figure 3a only shows the curve-fitting results for the spectrum at 10 min. Four bands at 1333, 1283, 1257 and 1221 cm^{-1} were obtained in the curve-fitting results. The correlation coefficients for all of the curve-fitting results were better than 0.996. Figure 3b shows the dynamic changes of the integrated area for these four bands.

As shown in Figure 3b, the integrated areas for these bands at initial time did not equal zero because the sample was exposed to reactant gases stream for 3 min before the spectra were collected in a closed system. The integrated area for the band at 1333 cm^{-1} changed invisibly. As discussed above, if this band is attributed to v_s(OCO) of $HSCO_2^-$ on MgO as a reaction intermediate, its intensity should decrease obviously with time in a closed system after a maximum was reached. On the other hand, gaseous SO_2 were also detected by MS in our previous work.[12] Therefore, it is more reasonable to assign this band (1333 cm^{-1}) to SO_2 than $HSCO_2^-$. The integrated area for the δ(COH) band of HCO_3^- (at 1221 cm^{-1}) increased obviously within the initial 10 min and then decreased slightly. It should be noted that the integrated area of gaseous CO_2 in Figure 1b kept a low increasing rate after 10 min, which means gaseous CO_2 might come from the decomposition of surface HCO_3^-. It was very interesting for the changes of integrated area of the band at 1283 cm^{-1}. It increased to a maximal value at 4 min, and then decreased obviously with time. The trend for the band at 1257 cm^{-1} was similar to the band at 1283 cm^{-1}, while the change rate and surface concentration of the band for 1257 cm^{-1} were lower than those for 1283 cm^{-1}. Obviously, if these bands belonged to surface carbonates or sulfate, their intensities should

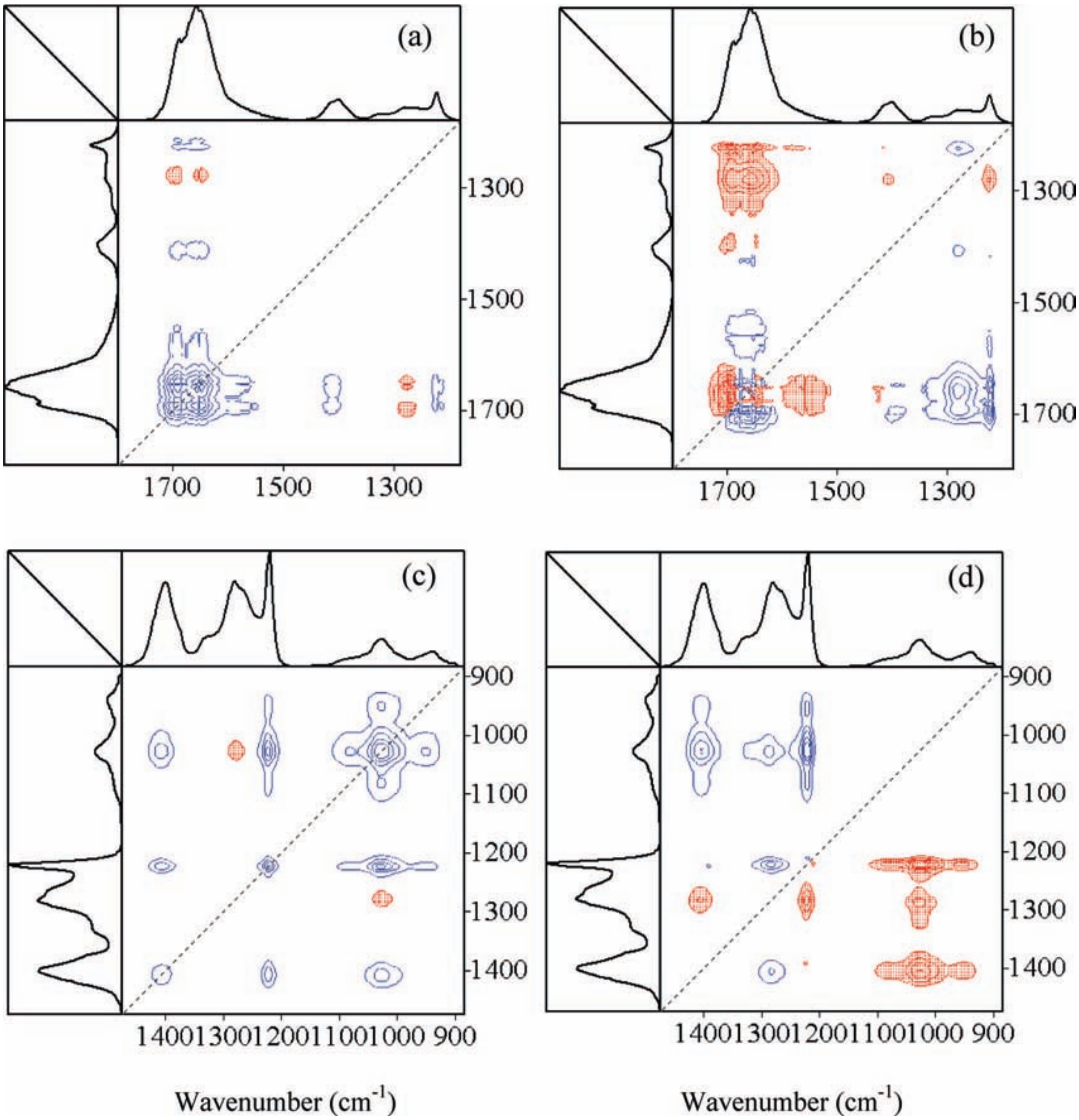

Figure 4. Two-dimensional correlation spectra for heterogeneous reaction of COS on MgO: (a) synchronous and (b) asynchronous in the range of 1150−1750 cm^{-1}; (c) synchronous and (d) asynchronous in the range of 900−1500 cm^{-1}. Blue color regions denote positive correlation in intensities, and red color regions denote negative correlation in intensities.

increase with time due to the increase of surface coverage, at least should not decrease with time.

Although the above analysis obtained more detailed information about the surface species, it was very difficult to discern temporal relationships among these surface species. In order to further clarify the correlation of these bands, two-dimensional correlation analysis was performed. Synchronous and asynchronous 2D correlation maps in the spectra region of 1150−1750 cm^{-1} are shown in parts a and b of Figure 4, while the synchronous and asynchronous maps 2D correlation in the region of 900−1500 cm^{-1} are shown in parts c and d of Figure 4. Blue color regions and red color regions denote positive and negative correlation in intensities, respectively. In Figure 4a, three strong autopeaks for ν(C=O) of H_2CO_3 (1693 cm^{-1}), ν_{as}(OCO) of HCO_3^- (1659 cm^{-1}) and δ(HOH) of H_2O (1632 cm^{-1}) were observed. It means their surface concentration increased significantly during the reaction time.[31,32] However, the intensities of the expected autopeaks at 1409, 1273, and 1225 cm^{-1} were invisible because their amplitudes of changes were much lower than that of the former three bands, while their corresponding cross-peaks were clearly visible. The positive region at 1409 and 1225 cm^{-1} in Figure 4a implies that they also increased during the reaction time, whereas the negative sign of the cross-peaks around 1273 cm^{-1} indicates its intensity decreased obviously. The cross-peaks in the range of 1500−1600 cm^{-1} which were assigned to carbonates also increased slightly. In the corresponding asynchronous plot (Figure 4b), the peak around 1400 cm^{-1} split into two components at 1404 and 1365 cm^{-1}. It was consistent with the result in the fourth derivative spectrum. In 2D correlation analysis, it is usually of advantage to scan only a section of the correlation map to pick up useful local features.[33] In this case, the band around 1273 cm^{-1} is of great interest. According to the rules of 2D correlation spectra,[31] it can be seen in Figure 4b that the bands around 1273 cm^{-1} varied prior to the bands attributed to HCO_3^- (1659, 1409, and 1221 cm^{-1}) and H_2CO_3 (1693 cm^{-1}), which implies the band around 1273 cm^{-1} was not related to HCO_3^- and H_2CO_3. In Figure 4, parts c and d, the variation of the band around 1273 cm^{-1} was also opposite in change direction to the bands in the range of 900−1200 cm^{-1}, which demonstrates that the band around 1273 cm^{-1} did not attribute to surface sulfate or sulfite. Therefore, the band around 1273 cm^{-1} (1280 and 1253 cm^{-1}) was most likely related to an intermediate ($HSCO_2^-$) on MgO.

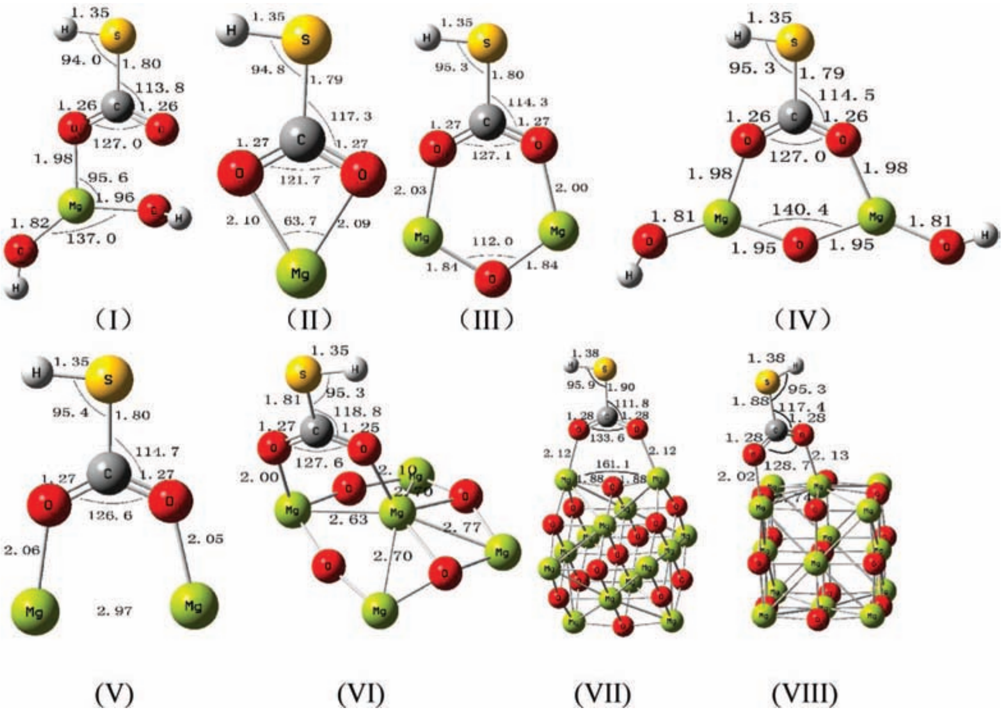

Figure 5. Energy minimized structures of HTCs on MgO. Models I−VI were optimized at the B3LYP/6-31+G(d,p) level of theory; Models VII and VIII were optimized at the B3LYP/6-31G level of theory. All bond lengths are given in angstroms and all angles are given in degrees.

3.3. Quantum Chemical Calculations for HTCs on MgO. To further confirm the assignment of the band around 1273 cm^{-1} and the structure of HTCs on MgO, several models were calculated at the B3LYP/6-31+G(d,p) level (Figure 5). Models I and II were built to represent monodentate and bidentate HTCs, respectively. Models from III to VI were constructed to represent bridged HTCs whose substrates were in different coordination environments. Model VI was built on the (100) surface of MgO based on the model V, while models VII and VIII were built on the (100) surface of three-layer slabs of MgO unit cells. As for models VII and VIII, it was too expensive for calculations at the B3LYP/6-31+G(d,p) level. Therefore, they were optimized at the B3LYP/6-31G level of theory. Stationary points were identified as true minima of the potential energy surface (PES) in all cases because no imaginary frequencies were found.

As shown in Figure 5, the bond lengths of S−H in models I−VI were equal to 1.35 Å, which was very close to that of HTC on Al_2O_3 (1.34 Å) calculated by Hoggan et al.[16] The bond lengths of C−S and C−O in above models were 1.80 (1.79−1.81) and 1.26 (1.25−1.27) Å, respectively. The bond lengths of C−S and C−O were significantly longer than that of HTC on Al_2O_3. The corresponding differences were 0.13 and 0.08 Å, respectively. However, as for model IV, its structure is very similar to that of bicarbonate on Al_2O_3 optimized by Baltrusaitis et al.[22] The bond length of C−O in bicarbonate was calculated to be 1.27 Å at the B3LYP/6-31+G(d,p) level,[22] which was almost equal to our results (1.25−1.27 Å). The bond length of Mg−O in models I−VI (1.98−2.10 Å) was also much longer than that of Al−O (1.76 Å[16]). This difference may result from the different methods in calculations and different substrates. However, the value calculated by us is equivalent to the bond length in crystal of MgO.[17] It means our result is reasonable.

It could also be seen in Figure 5 that the bond angles of HTCs were affected significantly by the structure of substrate. Bidentate HTC had the smallest angle of O−C−O (121.7 °), while the bond angles for monodentate and bridged HTCs were about 127°, which was very close to the bond angle of O−C−O in bicarbonate.[22] For bridged HTCs, the bond angle of O−Mg−O in model IV, in which one hydroxyl was added to each Mg atom, was much larger than that in model III. It means that the coordination environment of substrate greatly affects the structure of surface HTC. However, in the real crystal, the (100) face is the most stable face in periclase,[17] and the Mg atoms in the surface layer are 5-fold coordinated. Therefore, Mg−O−Mg in a real crystal should be much stiffer than that in models III and IV, and the bond angle of O−Mg−O in HTC should be larger than that in model III or model IV. In order to confirm this assumption, the bridged HTC was built on three-layer slabs of MgO unit cell (model VII) and the optimized geometry at the B3LYP/6-31G level of theory is shown in Figure 5. The angle of Mg−O−Mg was calculated to be 161.1° and that of O−C−O was 133.8°. They were much larger than the calculated values in models III and IV. Additionally, the distance of Mg−O−Mg in model IV was calculated to be 3.68 Å, while it is 4.21 Å for Mg−O−Mg in the (100) face of MgO crystal.[17] It suggests that the surface atoms in MgO crystal should reconstruct significantly when HTCs are formed on simple crystal edges (models III and IV), and a large energy barrier needs to be overcame for the formation of HTCs. Model V represents HTC formed on the two isolated Mg atoms. As shown in model V, when the distance between two Mg atoms was 2.97 Å, which is almost the same as that of Mg−Mg (2.98) in the (100) face of MgO crystal, the HTC has the lowest tension. Therefore, model V might be more feasible to be formed than models III and IV on the surface of a real MgO crystal because the formation of model V does not need a significant reconstruction of the MgO surface. As can be seen in Figure 5, the substrate in model VI which represents the bridged HTC on the (100) face of MgO crystal also distorted obviously. The center Mg atom departed from the plane by 0.93 Å, and the shortest distance of Mg−Mg was 2.63 Å, which was contrasted by 11.7% compared with that in the (100) face of the MgO crystal or model V. However, in model VIII which was optimized at the B3LYP/6-31G level, the distance between the

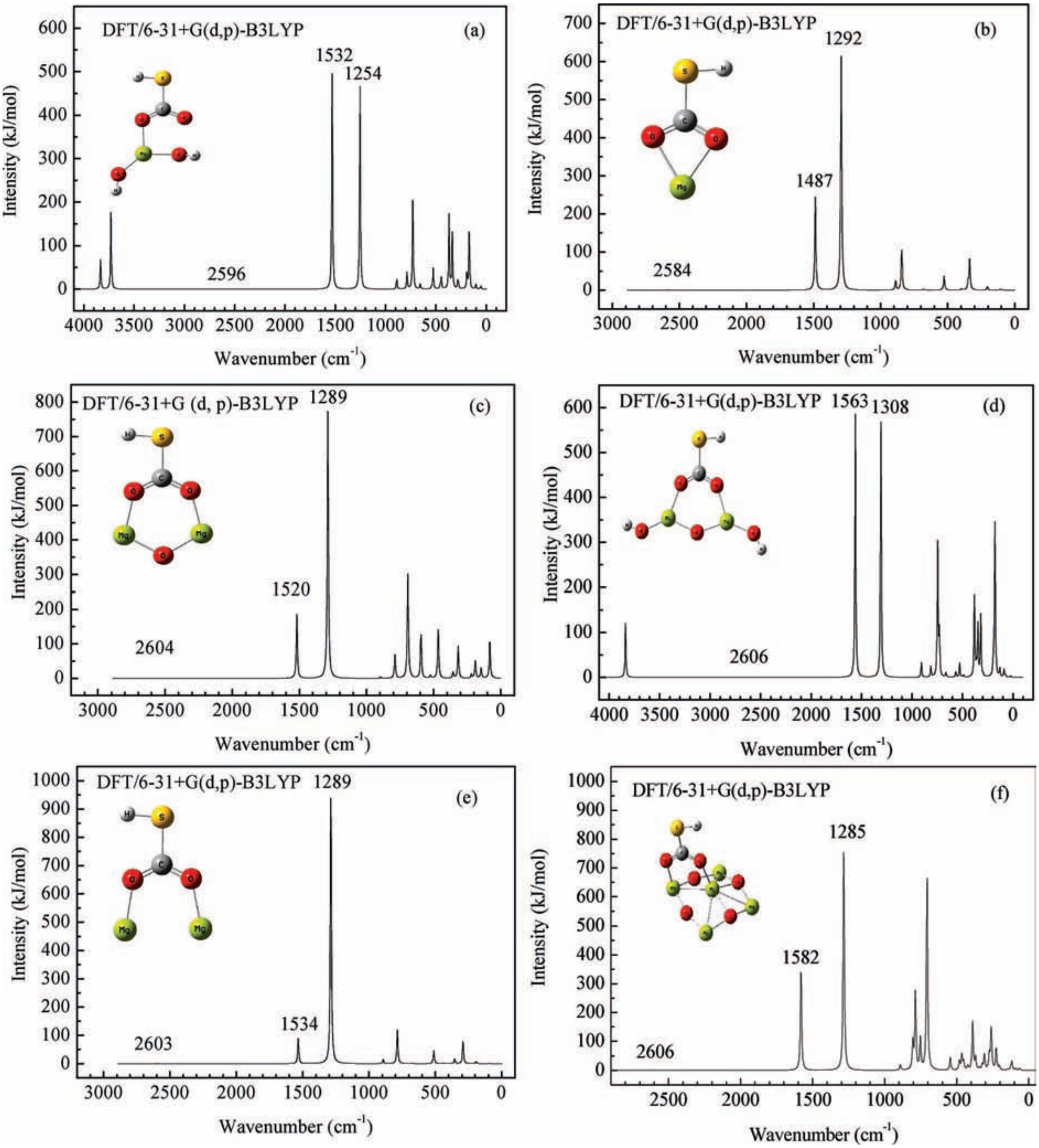

Figure 6. Calculated infrared spectra of HTCs. Frequencies were scaled to 0.9632.

first layer and the second layer was 2.49 Å, while that between the second layer and the third layer was 2.07Å. The degree of distortion was much lower than that in model VI. It demonstrates that in the real MgO crystal the reconstruction effect of surface atoms due to the formation of HTC should reduce greatly because the interaction of sublayer atoms. Therefore, when the crystal structure of MgO was considered, bridged HTC on the two neighboring Mg atoms (Mg−Mg) might be formed prior to that on Mg−O−Mg.

Figure 6 shows the calculated infrared spectra of HTCs on MgO at the B3LYP/6-31+G(d,p) level of theory. The frequencies were scaled to 0.9632.[27] In Figure 6, three characteristic absorption bands attributed to HTCs were observed. The very weak band at 2584−2606 cm^{-1} was assigned to υ(SH). The peaks at 1487−1582 and 1254−1308 cm^{-1} were υ_{as} and υ_{s} bands of O−C−O in the HTCs, respectively. The calculated υ_{s} bands were very close to the experimental value at 1283 and 1257 cm^{-1} in Figure 2. For example, as shown in Figure 6a, the frequency of υ_{s}(OCO) of monodentate HTC was calculated to be 1254 cm^{-1}. Compared with the band at 1257 cm^{-1}, the relative error for the frequency was 0.24%. The υ_{s}(OCO) band of bidentate HTC (Figure 6b) was calculated to be 1292 cm^{-1}. When compared with the band at 1283 cm^{-1}, the relative error was 0.70%. As for bridged HTCs shown in Figure 6c−f, except for model IV (Figure 5), the calculated frequencies for υ_{s}(OCO) were in the range of 1285−1289 cm^{-1}, which were very close to experimental value of 1283 cm^{-1} in Figure 2, and had very low relative errors from 0.16% to 0.48%. Especially, for model VI the calculated frequency was almost equal to the experimental value. As discussed above, bridged HTC is more feasible formed on the Mg−Mg site than on the Mg−O−Mg site in the (100) surface of MgO. Therefore, the band at 1283 cm^{-1} in Figure 2 should be assigned to υ_{s}(OCO) of bridged HTC which formed on the two neighboring Mg atoms, while the band at

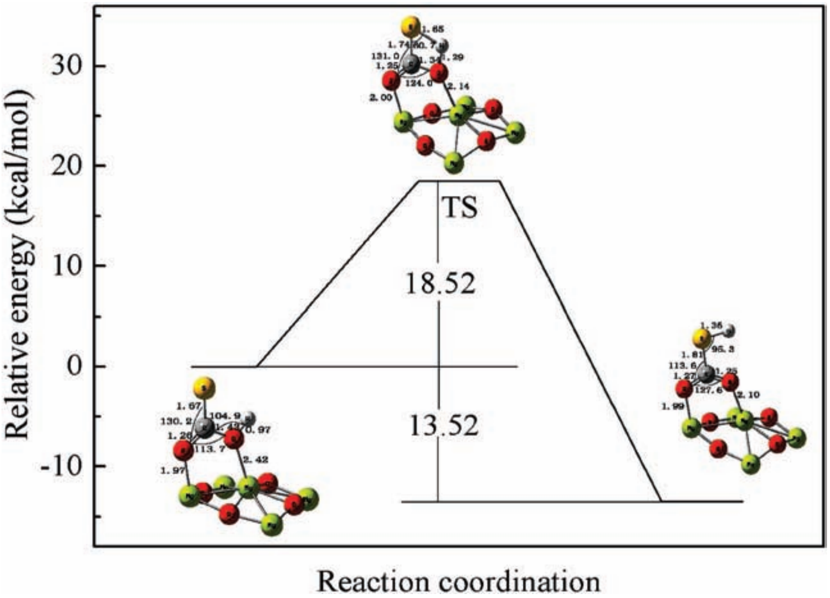

Figure 7. Calculated energetic diagram for the proton-transfer reaction of HTC at B3LYP/6-31+G(d,p) level of theory. All bond lengths are given in angstroms and all angles are given in degrees.

1257 cm^{-1} was the ν_s(OCO) band of the monodentate HTC. Of course, although models VII and VIII are more representative than the others in the real crystal, we did not calculate their corresponding infrared spectroscopy due to the high cost of computation at B3LYP/6-31+G(d,p) level.

It should be noted that if the bands at 1257 and 1283 cm^{-1} were related to the ν_s(OCO) band of HTC on MgO, the corresponding ν_{as}(OCO) and ν_s(SH) bands should also be observed in experiments. Although the bands at 1578, 1523, and 1497 cm^{-1} were also observed in Figure 2, their intensities changed in opposite direction with the bands around 1273 cm^{-1} (Figure 4a). In other words, as discussed in section 3.2, only the bands at 1283 and 1257 cm^{-1} had the features of intermediate. It needs to be pointed out that the calculated intensities of ν_{as} bands were much lower than that of ν_s bands for most of the HTCs in Figure 6. This was especially true for models II, III, V, and VI. On the other hand, as discussed in section 3.1, the accumulation of carbonates led to the increase in intensities in the region of 1520−1582 cm^{-1}. Therefore, it is hard to discern the very weak decrease for the ν_{as} band of HTCs due to the increase of surface carbonates in experiments. Additionally, the calculated frequencies for ν(SH) of HTCs were in the region of 2584−2606 cm^{-1}. In Figure 1a, a band at 2578 cm^{-1}was observed. However, it is more reasonable to ascribe this band to ν(SH) of surface HS because gaseous H_2S was detected in our previous work[14] and the intensities of ν(SH) in HTCs were almost invisible.

On the basis of isotope experiments, Baltrusaitis et al.[22] proposed that the formation of bicarbonate involves a nucleophilic attack of adsorbed CO_2 by surface OH groups followed by an intramolecular proton transfer on the surface. In other words, the oxygen atom in O−H of bicarbonate originates from that in CO_2. In our previous work,[10−12] we also proposed that the adsorbed COS was nucleophilic attacked by surface OH groups. As proposed by Hoggan et al.,[16] the S−H group but not the O−H group was formed in HTCs. Our calculations also supported this assumption. It means that the hydrogen atom must also be transferred from surface O−H groups to sulfur atom via an intermolecular proton transfer. Therefore, the energetics for the intramolecular proton transfer were calculated at the B3LYP/6-31G+(d,p) level of theory. All transition states were identified by the presence of one imaginary frequency.

Figure 7 shows the calculated energy diagram for the formation of HTC shown as model VI (Figure 5). The energies were calculated relative to the initial structure following O−H nucleophilic attack on a neighboring preadsorbed COS molecule. Subsequently, a hydrogen atom transferred from the O−H group to a sulfur atom of preadsorbed COS. The calculated activation energy for the transition state was 18.52 kcal·mol,$^{-1}$ and the product of this proton-transfer reaction of bridged thiocarbonate was energetically favored by 13.52 kcal·mol^{-1} at the B3LYP/6-31G+(d,p) level of theory with respect to the initial structure. Compared with the similar reaction for the formation of bicarbonate,[22] the activation energy for the proton-transfer reaction of HTC formation is much lower than that for bicarbonate on Al_2O_3, while the stabilization energies of bridged thiocarbonate is equivalent to that of bridged bicarbonate.

4. Conclusions

The broad band around 1273 cm^{-1} which was observed in in situ DRIFTS experiments for the heterogeneous reaction of COS on MgO was found to contain two bands at 1283 and 1257 cm^{-1} and had the typical features of intermediates. It was confirmed to be the ν_s band of HTCs using derivative spectroscopy analysis, 2DCOS analysis, and DFT calculations. The band at 1283 cm^{-1} was the ν_s(OCO) band of bridged HTC which formed on the two neighboring Mg atoms in the (100) face of MgO crystal. The band at 1257 cm^{-1} belonged to the ν_s(OCO) band of monodentate HTC on MgO. The change in intensity of ν_{as}(OCO) of HTCs was invisible in experiment due to the weak absorbance and the interruption of surface carbonates. Similar to the formation of bicarbonate on mineral oxide, the formation of HTCs occurred via a nucleophilic attack of preadsorbed COS by surface O−H groups followed by proton transfer from the O−H group to sulfur atom of preadsorbed COS. The activation energy for the transition state of intramolecular proton-transfer reaction of bridged thiocarbonate was calculated to be 18.52 kcal·mol^{-1} at the B3LYP/6-31+G(d,p) level of theory. The results in this study further confirmed the formation of thiocarbonate and provided more detail for the heterogeneous reactions of COS on mineral dust, which will help for understanding the chemical cycle of COS.

Acknowledgment. This research was funded by the National Natural Science Foundation of China (40775081, 50621804) and the Ministry of Science and Technology, China (2007CB407301).

References and Notes

(1) Crutzen, P. J. *Geophys. Res. Lett.* **1976**, *3*, 73–76.

(2) Chin, M.; Davis, D. D. *J. Geophys. Res.* **1995**, *100* (DS), 8993–9005.

(3) Watts, S. F. *Atmos. Environ.* **2000**, *34*, 761–799.

(4) Kettle, A. J.; Kuhn, U.; von Hobe, M.; Kesselmeimer, J.; Andreae, M. O. *J. Geophys. Res* **2002**, *107*, 4658–4675.

(5) Montzka, S. A.; Calvert, P.; Hall, B. D.; Elkins, J. W.; Conway, T. J.; Tans, P. P.; Sweeney, C. *J. Geophys. Res.* **2007**, *112*, D09302.

(6) Jacob, D. J. *Atmos. Environ.* **2000**, *34*, 2131–2159.

(7) Dentener, F. J.; Carmichael, G. R.; Zhang, Y.; Lelieveld, J.; Crutzen, P. J. *J. Geophys. Res.* **1996**, *101*, 22869–22889.

(8) Wu, H. B.; Wang, X.; Cheng, J. M.; Yu, H. K.; Xue, H. X.; Pan, X. X.; Hou, F. Q. *Chin. Sci. Bull.* **2004**, *49*, 1231–1235.

(9) Wu, H. B.; Wang, X.; Cheng, J. M. *Sci. China, Ser. B: Chem.* **2005**, *48*, 31–37.

(10) He, H.; Liu, J. F.; Mu, Y. J.; Yu, Y. B.; Chen, M. X. *Environ. Sci. Technol.* **2005**, *39*, 9637–9642.

(11) Liu, J. F.; Yu, Y. B.; Mu, Y. J.; He, H. *J. Phys. Chem. B* **2006**, *110*, 3225–3230.

(12) Liu, Y. C.; He, H.; Xu, W. Q.; Yu, Y. B. *J. Phys. Chem. A* **2007**, *111*, 4333–4339.

(13) Liu, Y. C.; Liu, J. F.; He, H.; Yu, Y. B.; Xue, L. *Chin. Sci. Bull.* **2007**, *52*, 2063–2071.

(14) Liu, Y. C.; He, H.; Mu, Y. J. *Atmos. Environ.* **2008**, *42*, 960–969.

(15) Liu, Y. C.; He, H.; Ma, Q. X. *J. Phys. Chem. A* **2008**, *112*, 2820–2826.

(16) Hoggan, P. E.; Aboulayt, A.; Pieplu, A.; Lavalley, J. C. *J. Catal.* **1994**, *149*, 300–306.

(17) Al-Abadleh, H. A.; Grassian, V. H. *Surf. Sci. Rep.* **2003**, *52*, 63–161.

(18) Turek, A. M.; Machs, I. E.; DeCania, E. *J. Phys. Chem.* **1992**, *96*, 5000–5007.

(19) Al-Hosney, H. A.; Grassian, V. H. *J. Am. Chem. Soc.* **2004**, *126*, 8068–8069.

(20) Karin, F.; Robert, S.; Günther, R. *Chem. Commun.* **2008**, 320–322.

(21) Doodsel, A. J.; Low, M. L. D.; Takezawa, N. *Environ. Sci. Technol.* **1972**, *6*, 268–273.

(22) Baltrusaitis, J.; Jensen, J. H.; Grassian, V. H. *J. Phys. Chem. B* **2006**, *110*, 12005–12016.

(23) Datta, A.; Cavell, R. G.; Tower, R. W.; George, Z. M. *J. Phys. Chem.* **1985**, *89*, 443–449.

(24) Schneider, W. F.; Li, J.; Hass, K. C. *J. Phys. Chem. B* **2001**, *105*, 6972–6979.

(25) Katsumoto, Y.; Adachi, D.; Sato, H.; Ozaki, Y. *J. Near Infrared Spectrosc.* **2002**, *10*, 85–91.

(26) Frisch, M.; Foresman, J.; Frisch, A. et al. Gaussian 98; Gaussian Inc.: Pittsburgh, PA, 1998.

(27) Irikura, K. K.; Johnson, R. D., III; Kacker, R. N. *J. Phys. Chem. A* **2005**, *109*, 8430–8437.

(28) John, A. P.; Richard, S. J.; Kennth, W. W. E.; Peter, R. G.; Gao, H. J. *Anal. Chem.* **1990**, *62*, 477–484.

(29) Goodman, A. L.; Bernard, E. T.; Grassian, V. H. *J. Phys. Chem. A* **2001**, *105*, 6443–6457.

(30) Wu, Q.; Gao, H. W.; He, H. *J. Phys. Chem. B* **2006**, *110*, 8320–8324.

(31) Noda, I. *Appl. Spectrosc.* **1993**, *47*, 1329–1333.

(32) Guo, Y.; Peng, Y.; Wu, P. Y. *J. Mol. Struct.* **2008**, *875*, 486–492.

(33) Ayora-Canada, M. J.; Lendl, B. *Vib. Spectrosc.* **2000**, *24*, 297–306.

JP809887C